

# RSC Advances



This is an *Accepted Manuscript*, which has been through the Royal Society of Chemistry peer review process and has been accepted for publication.

*Accepted Manuscripts* are published online shortly after acceptance, before technical editing, formatting and proof reading. Using this free service, authors can make their results available to the community, in citable form, before we publish the edited article. This *Accepted Manuscript* will be replaced by the edited, formatted and paginated article as soon as this is available.

You can find more information about *Accepted Manuscripts* in the [Information for Authors](#).

Please note that technical editing may introduce minor changes to the text and/or graphics, which may alter content. The journal's standard [Terms & Conditions](#) and the [Ethical guidelines](#) still apply. In no event shall the Royal Society of Chemistry be held responsible for any errors or omissions in this *Accepted Manuscript* or any consequences arising from the use of any information it contains.



Journal Name

ARTICLE

## Interlocked dimerization of $C_3$ -Symmetrical Boron Difluoride Complex: Designing Non-Cooperative Supramolecular Materials for Luminescent Thin Films

Received 00th January 20xx,  
Accepted 00th January 20xx

DOI: 10.1039/x0xx00000x

www.rsc.org/

Shigesaburo Ogawa,<sup>a</sup> Masa-aki Morikawa,<sup>b</sup> Gergely Juhász,<sup>a</sup> and Nobuo Kimizuka<sup>a,b\*</sup>

A lipophilic complex with radially-connected three  $\beta$ -diketonate boron difluoride ( $BF_2dk$ ) units to a central benzene ring was newly developed. The  $C_3$ -symmetrical  $BF_2dk$  complex (**1**) formed a self-complementary interlocked dimer (**1**)<sub>2</sub> with increasing concentration in  $CHCl_3$  as revealed by NMR spectroscopy and quantum chemical calculations. A remarkable luminescence color change from blue to yellow was observed in response to the formation of interlocked dimers. Electrostatic interactions, hydrogen bonding between negative convexes ( $BF_2$  moiety) and positive concaves (three protons aligned on each arms) principally contribute to the dimerization, whereas the formation of interlocked dimers was accompanied by conformational changes of constituent molecules which interrupted further association. Consequently, casting of the chloroform solution of interlocked dimers on solid supports gave uniform thin films without uneven crystallization. It provides a new perspective of designing anti-cooperative systems for homogeneous molecular coatings.

### Introduction

Self-assembly of photofunctional molecules has been attracting much interest as a means to create nanoarchitectures and their cooperative functions that are not accessible from the constituent molecules.<sup>1</sup> Amphiphilic molecular design is widely adopted to achieve self-assembly of functional molecules in aqueous, organic and ionic media.<sup>2</sup> In general, increase in the concentration of unit molecules cause extended aggregation into developed structures,<sup>1</sup> which are indispensable to achieve stand-alone supramolecular functions in given solvent media. In particular, formation of ordered aggregates in crystalline order has been preferred to achieve photofunctionalities such as long-range transfer of photon energy or charge carriers. On the other hand, in nanotechnology fields such as photovoltaics, photochemical events at the interface are of crucial importance. There exist strong demands for photofunctional molecular systems that evenly and densely spread on surfaces as homogeneous functional molecular coatings. Such molecular systems preferably show adaptive nature to varied surfaces, which needs to be designed from a different perspective from the widely-received highly-ordered self-assembly under thermodynamic equilibrium. That is, there are two issues to be

solved. First, uniform thin films need to be facily obtained by casting or spin coating method, which require inhibition of crystal nucleation in the kinetically controlled solvent evaporation processes, i.e., under far-from-equilibrium conditions. Second, to meet the above requirement, a molecular design principle is required to accumulate photofunctional units in high density while avoiding their extended aggregation in solution.

To avoid the formation of crystalline aggregates in solution, the simplest approach is to design suitably designed molecules that preferentially form dimers which do not further assemble to extended aggregates.



This is the case that the dimerization constant  $K$  is much larger than that for subsequent aggregation, which is referred to as anti-cooperative process.<sup>1</sup> Although this process has received much less attention, it can be realized for example in aggregation of structurally flexible  $\pi$ -systems with peripheral alkyl chains, where dimerization induces changes in the conformation and orientation of alkyl chains to turn away to the other side of  $\pi$ -faces. Such dimerization-induced steric interaction between aliphatic side chains may consequently lead to the interruption of further association.

With this view in mind, we have designed a  $C_3$ -symmetrical boron difluoride  $\beta$ -diketonate ( $BF_2dk$ ) complex in expectation of the formation of dimers which do not further aggregate in solution. Among varied molecular architectures developed so far, radial integration of functional units provides a means to introduce multiple photofunctional groups in a unit molecule, which is advantageous to enhance the density of these

<sup>a</sup> Department of Chemistry and Biochemistry, Graduate School of Engineering, Kyushu University, 744 Moto-oka, Nishi-ku, Fukuoka, 819-0395 (Japan)

<sup>b</sup> Center for Molecular Systems (CMS), Kyushu University, 744 Moto-oka, Nishi-ku, Fukuoka, 819-0395 (Japan). Tel +81-92-802-2832, Fax +81-92-802-2838, e-mail : n-kimi@mail.cstm.kyushu-u.ac.jp

Electronic Supplementary Information (ESI) available: [details of any supplementary information available should be included here]. See DOI: 10.1039/x0xx00000x

functionalities even in the condensed state. For example, molecules with  $C_3$ -symmetrical axis have been widely studied in liquid crystals,<sup>3</sup> supramolecular polymers<sup>4</sup> and biomolecule-conjugates.<sup>5</sup> On the other hand, the family of  $BF_2dk$  complexes has been attracting much interest due to their unique properties as exemplified by large molar absorption coefficients,<sup>6a</sup> large ground dipole moment ( $\mu = 6.7$  Debye for  $BF_2$  dibenzoylmethane complex),<sup>6b</sup> high emission quantum yields,<sup>6c,6d</sup> two-photon absorption,<sup>6a</sup> efficient electron transport<sup>6e</sup> and mechanochromic luminescence.<sup>6f</sup> The  $BF_2dk$  complexes have been also introduced in molecular assemblies such as organogels,<sup>7</sup> liquid crystals,<sup>6c,8</sup> nanoparticles<sup>9</sup> and self-assembled monolayers.<sup>10</sup> In these systems, however, the design of  $BF_2dk$  complexes that form discrete dimers with anti-cooperative nature has been unprecedented.

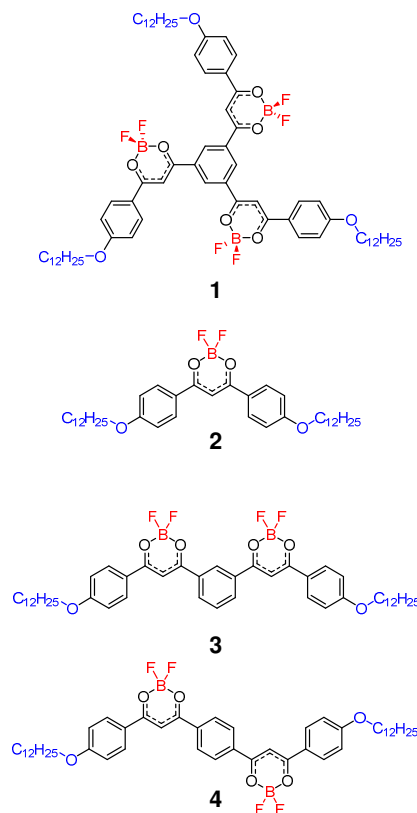
The design of a novel  $C_3$ -symmetrical molecular framework for  $BF_2dk$  complex **1** is shown in Scheme 1. Three  $BF_2dk$  units are radially integrated in a central phenyl ring with long alkyl chains to ensure solubility in common organic solvents. The dodecyloxy groups are introduced at the para-position of dibenzoylmethane groups, in expectation for enhancing luminescent quantum yields.<sup>6c</sup> The boomerang-shaped mono- $BF_2dk$  complex (**2**)<sup>6d,8b</sup> and linearly-connected di- $BF_2dk$  complexes (**3**, **4**)<sup>10b</sup> were synthesized as references in order to gain insight into the effect of molecular geometry on their intermolecular interactions, solubility and luminescence properties. Self-assembly of these complexes was examined in chloroform, and their accumulation on solid substrate was also investigated in terms of the development of homogeneous molecular coatings.

## Results and discussion

### 2.1. Spectroscopic characterization of $BF_2dk$ complexes in dilute solution.

The effect of molecular structures on the spectroscopic property of  $BF_2dk$  complexes (**1–4**) was measured in dilute solutions. Fig. S2 (ESI) shows UV-vis absorption spectra of the complexes **1–4** and the corresponding ligands **1L–4L** in chloroform (10  $\mu$ M, 20 °C). Chloroform was chosen as solvent because of its superior property to dissolve a wide range of molecules. Absorption peaks of the complexes are observed around at 410–430 nm, which are red-shifted from the corresponding ligands ( $\lambda_{max}$  at 365–390 nm) due to coordination of  $\beta$ -diketonate groups to  $BF_2$ .<sup>6b</sup> In luminescence spectra, the complexes **1–3** showed blue luminescence at 440–450 nm whereas complex **4** gave cyan-colored luminescence at 480 nm (Fig. S3 and Table S1, ESI).

All the  $BF_2dk$  complexes showed high emission quantum yields ( $\Phi_e$ ) above 88 %, which are consistent with those reported for  $BF_2dk$  derivatives possessing electron donating groups in the para positions.<sup>6c</sup>  $^1H$ -NMR spectra were obtained for the  $BF_2$  complexes and ligands, whose chemical shifts for the aromatic and enolic protons were summarized in Tables S2 and S3 (ESI). The ligands **1L–4L** in dilute  $CDCl_3$  solution showed a singlet signal at ca. 17.0 ppm, which are assignable to enolic



Scheme 1. Molecular structure of lipophilic  $BF_2dk$  complexes **1–4**.

protons of  $\beta$ -diketonate groups. The keto methylene protons were not observed, indicating that the enol tautomer is the dominant form in chloroform. Meanwhile, in  $BF_2dk$  complexes the enolic proton signals disappeared completely even for diluted solutions (10  $\mu$ M), reflecting the stability of  $BF_2$  complexes. The chemical shifts of the aromatic protons in  $BF_2dk$  complexes showed remarkable downfield shifts compared to those observed for the corresponding ligands **1L–4L**, reflecting electron withdrawal by the  $BF_2$  units. It is also to note that the trigonal complex **1** showed aromatic protons most downfield shifted at among all compounds tested in this study. This is ascribable to formation of intermolecular  $B-F \cdots H$  hydrogen bonding in the  $C_3$ -symmetrical complex **1** in organic media; the aromatic protons serve as hydrogen bond donors and  $BF_2$  units as acceptors, as discussed below.

### 2.2. Self-assembly characteristics of $BF_2dk$ complexes.

The solubility of  $BF_2dk$  complexes in chloroform is amenable to change depending on the chemical structure. The serially-concatenated complexes **3** and **4** show high crystallinity and were poorly soluble in chloroform. Micrometer-sized precipitates were formed upon standing the heat-dissolved 1.0 mM solutions at ambient temperature. In contrast, compounds **1** and **2** showed superior solubility and were

homogeneously dissolved in chloroform. The formation of aggregates was characterized by a dynamic light scattering (DLS). The concentration dependence of the DLS count rate for the complex **1** showed apparent deviation from the linear relationship above *ca.* 1.0 mM, which is consistent with the formation of the molecular assembly (Fig. S4, ESI). Correspondingly,  $^1\text{H}$ -NMR spectra of the complex **1** showed considerable upfield shifts in the aromatic protons of  $\text{H}_b$ ,  $\text{H}_c$ , and  $\text{H}_d$  above the concentration of *ca.* 1.0 mM (Fig. 1a, c). The observed gradual upfield shifts in aromatic protons indicate that the  $\text{C}_3$ -symmetric complex **1** forms parallel stacked aggregates which are in equilibrium with monomeric species on the  $^1\text{H}$ -NMR time scale. As shown in Fig. 1 inset, upon increasing the concentration of **1**, the DLS diameter gradually increased from  $1.66 \pm 0.24$  nm (3 mM) to  $2.42 \pm 0.31$  nm (24 mM). These values indicate that the equilibrium consists of monomeric and small discrete aggregates and do not involve the formation of extended aggregates in solution. The VPO measurement showed that the complex **1** existed as monomers below the concentration of 1.0 mM. The number average molecular weight of **1** showed increase with the increase of concentration, which is explicable by the formation of dimeric aggregates (Fig. S6, ESI). The complexation of ligand **1L** with  $\text{BF}_2$  unit promotes the formation of dimers, as the trigonal ligand **1L** alone showed upfield shifts only above the high concentration of  $\sim 10$  mM (Fig. S5a, ESI). In the case of **2**, however the spectral shifts were observed above the higher concentration of 50 mM (Fig. S5b, ESI), and thus the mono- $\text{BF}_2\text{dk}$  complex **2** has lower tendency to form aggregates in solution.

The contribution of  $\text{B-F}\cdots\text{H}$  hydrogen bonding in the self-assembly of complex **1** was then investigated by  $^{19}\text{F}$ -NMR spectroscopy. The fluorine signal of **1** showed presence of a satellite peak component derived from the naturally-abundant 19.58%  $^{10}\text{B}$  ( $I = 3$ ) isotope (Fig. 1b).<sup>11</sup> A broad peak was observed for  $\text{BF}_2\text{dk}$  complex, which would be ascribed to the fast relaxation influenced by the quadrupolar boron nucleus.<sup>12</sup> As can be seen in Fig. 1d, the fluorine signal of the complex **1** is concentration-dependent and showed downfield shift above the concentration of *ca.* 1.0 mM. This concentration threshold coincides with that observed for the upfield shifts of aromatic protons in  $^1\text{H}$ -NMR measurements, and these observations are indicative of the formation of intermolecular  $\text{B-F}\cdots\text{H}$  hydrogen bonding in the aggregates formed.<sup>13</sup> Pseudo-association constants  $K_2$  were then determined for **1** and **1L** based on the concentration dependence of the  $^1\text{H}$ - and  $^{19}\text{F}$ -NMR chemical shifts. The dimer model was adopted since the formation of dimer as unit assembly is supported by vapor pressure osmometry (VPO) as described above and the quantum chemical calculation. The nonlinear least-squares fitting to eq. 1 (Experimental Section)<sup>14</sup> was carried out to determine  $K_2$  values in  $\text{CDCl}_3$  at 20 °C and 30 °C (solid line in Fig. 1c, d). The averaged  $K_2$  value calculated from  $^1\text{H}$ - and  $^{19}\text{F}$ -NMR data are  $27.0 \text{ M}^{-1}$  at 20 °C and  $25.0 \text{ M}^{-1}$  at 30 °C, respectively.

A  $K_2$  value of  $45.2 \text{ M}^{-1}$  was obtained by VPO at 30 °C, which is basically consistent with that obtained from NMR ( $K_2 = 25.0 \text{ M}^{-1}$  at 30 °C) where the observed variance in two different

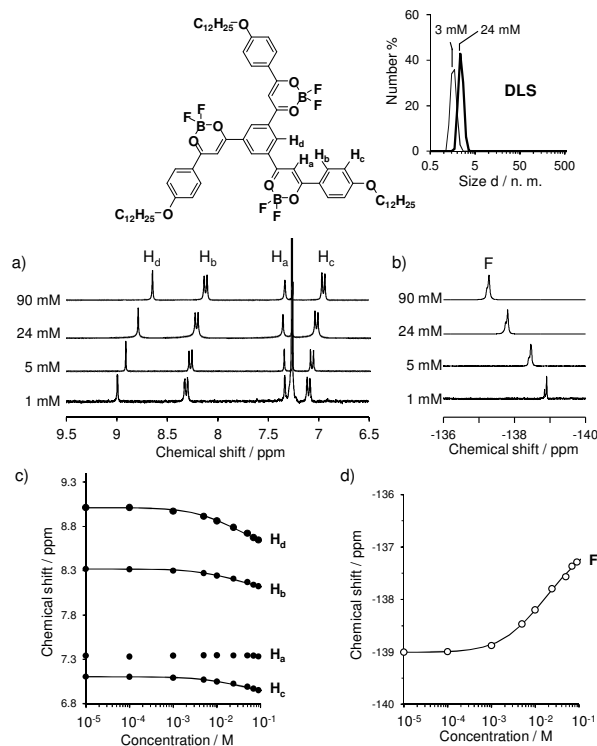


**Fig. 1** Concentration dependence of proton and fluorine signals in NMR measurements in  $\text{CDCl}_3$  at 20 °C. (a)  $^1\text{H}$ - and (b)  $^{19}\text{F}$ -NMR spectra of the complex **1** at varied concentrations. Changes in chemical shifts of (c) aromatic protons ( $\text{H}_a$ ,  $\text{H}_b$ ,  $\text{H}_c$  and  $\text{H}_d$ ) and (d) fluorine in the complex **1** as a function of the concentration. The circles indicate the experimental values and the solid lines indicate the calculated profile according to eq. 1. Inset, DLS size distribution curves of complex **1** in chloroform.

measurements is inherent in weak aggregation systems.<sup>2c</sup> Meanwhile, the association constant for **1L** was determined to be less than  $1.0 \text{ M}^{-1}$  at 20 °C (Table S4, ESI). From these results, it is apparent that the radially-connected three  $\text{BF}_2$  units play an essential role for the formation of dimeric self-assembly in chloroform.

### 2.3. Molecular geometry and electric potential surface of the $\text{C}_3$ -symmetrical core unit.

Quantum chemical calculations were further conducted to elucidate the intermolecular interactions in dimers of **1** and the role of core moiety. The details of the calculations are described in ESI. In the calculations, the dodecyloxy substituents in the complex **1** were omitted for simplification. The optimized structure of the monomer of **1** is shown in Fig. 2a. The radial orientation of  $\text{BF}_2\text{dk}$  complexes with  $\text{C}_3$ -symmetrical axis is shown to be the most stable conformation as compared to the other structural isomer by  $5.18 \text{ kcal}\cdot\text{mol}^{-1}$ , indicating the complex **1** adopt nearly a planar structure in solution (Fig. S7, ESI). The electric potential surface of **1** (Fig. 2b) shows positive concaves and negative convexes, which are formed on each arm of the molecule. The negative convex is due to the  $\text{BF}_2$  moiety, which serves as hydrogen bond acceptors and the positive concave is given by the series of  $\text{H}_a$ -

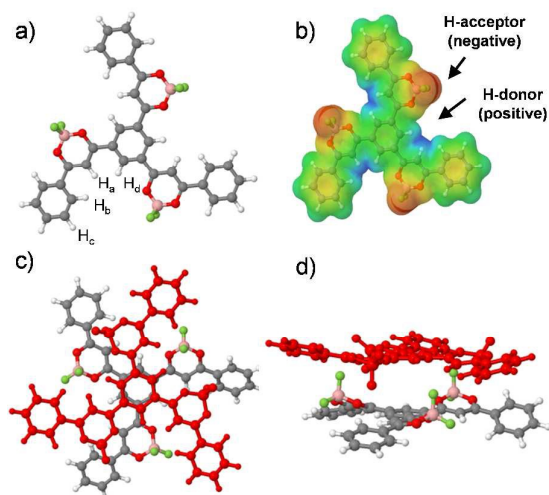


**Fig. 2** (a) Geometry, (b) electric potential surface of the core unit, and (c,d) geometry of the interlocked dimer formed between two core units of the model compound from top and side views.

$H_b$ - $H_d$  atoms. Interestingly, the electrostatic interactions and formation of H-bonds formed interlocked dimer ( $1$ )<sub>2</sub> (Fig. 2c, d) with an interaction energy of  $24.49 \text{ kcal}\cdot\text{mol}^{-1}$ . This energy is much larger than that of regular  $\pi$ - $\pi$  stacking, which is generally in order of  $1.5$ – $2.5 \text{ kcal}\cdot\text{mol}^{-1}$ . While the parallel alignment of the central rings in the dimer allows  $\pi$ - $\pi$  stacking, the arms of the molecules are rotated to alleviate steric hindrance and to maximize Coulombic interactions and H-bonds.

The average distances between  $H_a$ ,  $H_b$ ,  $H_d$  atoms and a fluorine atom in  $\text{BF}_2\text{dk}$  complex are shown in Table S5 (ESI):  $\text{B-F}\cdots\text{H}_a = 2.484 \text{ \AA}$ ,  $\text{B-F}\cdots\text{H}_b = 2.248 \text{ \AA}$  and  $\text{B-F}\cdots\text{H}_d = 2.978 \text{ \AA}$ . The angle between B-F and  $\text{F}\cdots\text{H}$  bonds is approximately  $120^\circ$  ( $120.4^\circ$  ( $H_a$ ),  $118.0^\circ$  ( $H_b$ ) and  $125.8^\circ$  ( $H_d$ ), Table S6, ESI). In this dimer geometry, the strongest interaction is expected between the F atom and  $H_b$ , which is in line with the observed  $^1\text{H-NMR}$  shifts as discussed in the previous section. The dimerization requires conformational changes in  $1$ , that is, rotation of the  $\text{BF}_2$  groups toward the neighbouring molecule. It makes one F atom of the  $\text{BF}_2$  to adopt an “equatorial position” and the other one pointing toward the donor groups of the neighbouring molecules (Fig. 2d). The intermolecular distance in this dimer geometry is around  $4.0 \text{ \AA}$ , which is a general figure since the aromatic rings are not perfectly orientated parallel (Fig. S8, ESI). This aggregation-induced conformational change of the core units would render alkyl chains on the periphery of this interlocked dimer turning a way towards non-aggregated faces of the dimeric core, and thus encumbered aggregation into further extended structures. Although the whole self-assembly is determined by contribution of each intermolecular force and solvophobic interactions to the total Gibbs free energy, the formation of this interlocked dimers is promoted by both the  $\text{B-F}\cdots\text{H}$  hydrogen bonding and Coulombic interactions, rather than the  $\pi$ - $\pi$  stacking.

## 2.4. Photoluminescence properties of interlocked dimers in solution and in cast films.

The photoluminescence characteristics associated with the formation of interlocked dimers were then investigated. Fig. 3a shows the change in UV-vis absorption spectra of the complex  $1$  as a function of the concentration in chloroform. As described before, the dilute  $10 \mu\text{M}$  solution gave a monomeric absorption peak at  $424 \text{ nm}$  (Fig. S2a, ESI), and similar spectrum was also observed for a  $1.0 \text{ mM}$  solution. Meanwhile, upon increasing the concentration, the spectral maximum showed a blue shift to  $408 \text{ nm}$  (concentration;  $24 \text{ mM}$ ). Such a blue-shift in absorption peak caused by self-assembly is generally ascribed to the excitonic interactions among transition dipole moments aligned in parallel geometry (H-aggregates).<sup>7a,15</sup> This parallel chromophore orientation is basically consistent with the structure of interlocked dimers ( $1$ )<sub>2</sub> with some rotational displacement as shown in Fig. 2.

In luminescence spectra, blue emission with a peak at  $450 \text{ nm}$  was observed for monomeric species (concentration; below  $1.0 \text{ mM}$ ). On the other hand, with increasing the concentration of  $1$  beyond  $1.0 \text{ mM}$ , a broad peak appeared around at  $560 \text{ nm}$ . Fig. 3c shows a dependence of  $I_{560}/I_{450}$ , the relative luminescence intensity at  $450$  and  $560 \text{ nm}$ , on the concentration of  $1$ . The red-shifted broad emission at  $560 \text{ nm}$  became dominant above the concentration of  $\sim 24 \text{ mM}$ . A full width at half maximum (fwhm) of  $122 \text{ nm}$  and a large Stokes shift of  $152 \text{ nm}$  are obtained from the emission spectrum recorded at  $46 \text{ mM}$ . Observation of such remarkably red-shifted emission spectra are often discussed in terms of excimers formed in the photorelaxation process.<sup>16</sup> Excimers are usually formed when an electronically excited molecule and a ground state molecule collide and come into specific and close contact each other, allowing excitation exchange interactions.<sup>17</sup> The photon emission from excimers is usually followed by molecular dissociation of the ground state molecules due to the  $\pi$ -orbital repulsion. In the case of  $1$ , the red-shifted yellow emission is observed above the critical aggregation concentration of  $1.0 \text{ mM}$ , and it is reasonably assigned to emission from the interlocked dimers existing in solution and not from typical excimers formed by diffusion and collision of chromophores. The presence of exciton interactions, i.e., delocalization of excitation energy in interlocked dimers ( $1$ )<sub>2</sub> was inferred from the blue-shifted UV-vis spectra (Fig. 3a). The interlocked dimers ( $1$ )<sub>2</sub> are formed in its ground state with the face-to-face separation distance of  $\sim 4 \text{ \AA}$  (Fig. 2d and Fig. S8, ESI), which is close to the equilibrium separation of excimers ( $\sim 4 \text{ \AA}$ ).<sup>17</sup> It is also possible that the structural distortion of chromophores caused by the formation of inter-locked dimers (Fig. 2) may also contribute to the observed fluorescence characteristics. Absolute photoluminescence quantum yield determined for the monomeric complex  $1$  was  $90 \%$  ( $1.0 \text{ mM}$ ), whereas it gradually decreased to  $46 \%$  in response to the formation of interlocked dimers ( $46 \text{ mM}$ , Fig. S9, ESI). Such a decrease in luminescence quantum yield is often observed for  $\pi$ -stacked aromatic chromophores.<sup>18</sup>

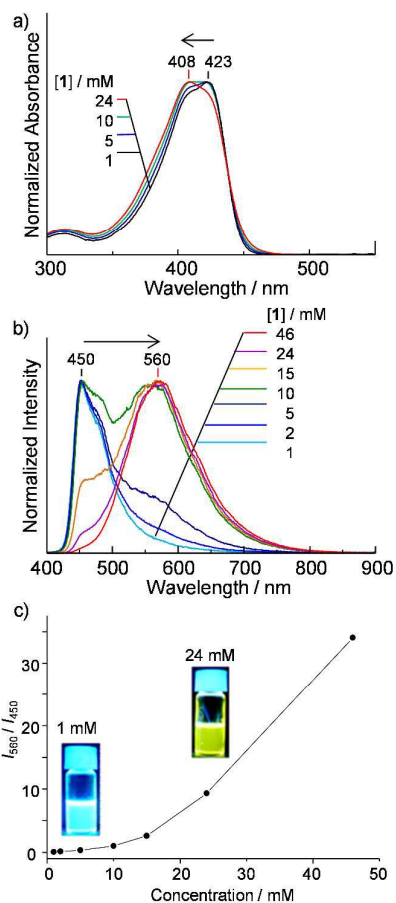


**Fig. 3** Concentration dependences of (a) absorption and (b) emission spectra of the complex **1** in chloroform ( $\lambda_{\text{ex}} = 365$  nm,  $20^\circ\text{C}$ ). (c) Dependence of relative luminescence intensity at 450 and 560 nm ( $I_{560}/I_{450}$ ) on the concentration of **1**. Inset shows photographs of the solutions (concentrations; 1 and 24 mM) under illumination by a UV lamp ( $\lambda_{\text{ex}} = 365$  nm).

To investigate if the interlocked dimers (**1**)<sub>2</sub> show anti-cooperative feature and do not show detectable crystallization even in the non-equilibrium solvent casting process, the morphology and luminescence of BF<sub>2</sub>dkcomplexes (**1–4**) were observed for cast films by using confocal laser scanning microscopy (CLSM). The samples were prepared by drop casting of chloroform solutions (1.0 mM) on quartz plates. Fig. 4a–d show CLSM images of the complexes **1–4** after removal of the solvent. In the case of the complexes **3** and **4**, micrometer-sized needle- or rod-like aggregates were already formed in chloroform and they were deposited on the substrates (Fig. 4c, d). The boomerang-shaped mono-BF<sub>2</sub>dk complex **2** also formed crystalline domains on the substrate after evaporation of the solvent (Fig. 4b). On the other hand, the complex **1** did not show such crystallization on the surface and gave a very uniform and homogeneous film (Fig. 4a). In X-ray diffraction (XRD) measurement, no apparent peaks were detected, indicating amorphous nature of the film (Fig. S10, ESI). These results clearly indicate that the dimer complex **1** does not readily form crystalline order aggregates on the

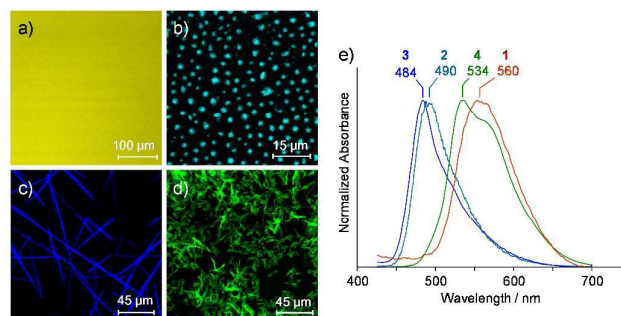


**Fig. 4** CLSM images of the solid state BF<sub>2</sub>dk complexes drop casted from a 1 mM chloroform solution of (a) **1**, (b) **2**, (c) **3**, and (d) **4**. The fluorescence images were obtained by excitation at 405 nm with a long-pass filter (420 nm). (e) Corresponding photoluminescence spectra of the complex **1–4** excited at 365 nm.

substrate during the solvent evaporation process. As described before, the radially attached solvophilic alkyl chains in the interlocked dimers (**1**)<sub>2</sub> tend to enclose the aromatic core and it must have effectively suppressed the formation of crystalline aggregates. The cast film of **1** showed an absorption peak at 398 nm and exhibited yellow emission centred at 560 nm (Fig. 4e) with a quantum yield of 40 %. The observed absorption peak is slightly blue shifted as compared to those observed for the inter-locked dimers in chloroform at higher concentrations (408 nm at 24 mM, Fig. 3a), the emission maximum of the film is essentially same as that observed for the interlocked dimer (**1**)<sub>2</sub> in solution. These observations confirm the validity of our approach to develop homogeneous photofunctional supramolecular coatings at the interface by taking advantage of the accumulation of interlocked dimers with anti-cooperative self-assembling characteristics. Although the crystallization of interlocked dimers is suppressed under the normal casting condition, powdery sample with lower crystallinity was obtained when the chloroform solution of **1** (1 mM, 1 liter) was slowly evaporated. It exhibited weak and broad diffraction peaks in the powder XRD measurement (Fig. S11, ESI). Thus, formation of crystalline aggregates is almost suppressed for interlocked dimers but not completely prohibited depending on the kinetic solvent removal conditions. Depending on the perspective under conventional thermodynamic equilibrium, the observed suppression of crystalline aggregate in solution could be classified into a specific monomer-dimer model.<sup>1b</sup> However from the view of developing homogeneous supramolecular coatings in the course of solution to solid phase changes, i.e., under non-equilibrium conditions, it would be helpful to classify the present system into the category of anti-cooperative self-assembly. The formation of interlocked lipophilic dimers (**1**)<sub>2</sub> is accompanied by conformational changes of the constituents which inhibit formation of extended crystalline aggregates in solution and even in the solvent-evaporation process. This anti-cooperative methodology with interlocked dimerization of C<sub>3</sub>-symmetrical functional units will find applications where homogeneous molecular coating with condensed functional groups are required.

## Experimental Section

**Materials.** All solvents used in this study are of analytical grade, and they are used as received. Sample solutions were prepared by dissolving the compounds in chloroform by heating to ca. 60 °C and subsequent ultra-sonication. The films were prepared on quartz plates by drop casting from the chloroform solution (1.0 mM).

**Characterization.**  $^1\text{H}$ - and  $^{19}\text{F}$ -NMR spectra were measured on an AVANCE 300 M Type 300MHz NMR (Bruker BioSpin Co., Ltd.) using  $\text{CDCl}_3$  as solvent. As external standards, tetramethylsilane (TMS) and 2, 2, 2-trifluoroethanol (−76.76 ppm) were used for  $^1\text{H}$ -NMR and  $^{19}\text{F}$ -NMR measurements, respectively.<sup>19</sup> UV-vis absorption spectra were recorded on a JASCO V-670 spectrometer. High concentration samples were measured with thin liquid films sandwiched by two quartz plates (liquid crystal cells, 6.8  $\mu\text{m}$  spacing). The excitation light was provided perpendicularly to the liquid films placed on a stage of optical microscope (Nikon ECLIPSE 80i) and luminescence spectra were obtained by using a photonic multichannel analyzer (Hamamatsu Photonics PMA-12) attached to the optical microscope at room temperature. Confocal laser scanning microscopy (CLSM) images were obtained by using a Carl Zeiss LSM510META excited with a blue diode laser at 405 nm. Absolute photoluminescence quantum yields were determined by absolute PL quantum yield measurement system (Hamamatsu Photonics, C9920-02) equipped with an integrating sphere instrument. The validity of the value was confirmed by using two standard solutions of acridine yellow in absolute ethanol ( $\Phi_E = 47\%$ ) and methanol ( $\Phi_E = 57\%$ ), respectively.<sup>20</sup> Dynamic light scattering (DLS) were measured by using the Malvern Zeta sizer Nano-ZS. Plot of mean count rate was obtained as the average values for 10 times measurements. Vapor pressure osmometry (VPO) was carried out on an OSMOMAT 070 (GONOTEC GmbH Co., Ltd.) using benzil (MW: 210.23) as a standard compound in chloroform at 30 °C. X-ray diffraction (XRD) measurement was performed on a Rigaku SmartLab diffractometer with Cu K $\alpha$  radiation ( $\lambda = 1.5406 \text{ \AA}$ ).

**Determination of association constant by  $^1\text{H}$  and  $^{19}\text{F}$ -NMR spectroscopies.** The pseudo-association constant  $K_2$  was calculated based on a dimer model described by Martin (eq. 1), where  $\delta$  is the observed chemical shift,  $\delta_{\text{monomer}}$  is the chemical shift of monomer,  $\Delta\delta$  is the difference in chemical shift between monomer ( $\delta_{\text{monomer}}$ ) and dimer ( $\delta_{\text{dimer}}$ ).  $K_2$  is the association constant for dimerization in  $\text{M}^{-1}$ ,  $C$  is the concentration of the sample, and  $L = K_2 C$ .<sup>14</sup> The chemical shifts versus concentration data were analyzed by nonlinear least squares fitting using Microsoft Excel 2010 Solver Add-In.

$$\delta = \delta_{\text{monomer}} - \Delta\delta(1 + (1 - \sqrt{8L + 1})/4L) \quad (\text{eq. 1})$$

**Quantum chemical calculation.** The calculations were carried out with B3LYP method and 6-311G(d) basis set using Gaussian 09 program (full citation is in the ESI). Default convergence criteria were used for the SCF calculations and

the geometry optimizations. The stability of the geometries and the possibility of alternative structures were checked with frequency calculations, as well as re-optimizing the geometry after random distortions along selected distortion angles, respectively.

## Conclusions

A lipophilic  $C_3$ -symmetric  $\text{BF}_2\text{dk}$  complex (**1**) that form interlocked dimers in organic media was developed. NMR spectroscopies and quantum chemical calculations revealed that the interlocked dimers are formed by electrostatic interactions between positive concaves and negative convexes of neighboring molecules, where H-bonds between the fluorine and aromatic protons play important roles. Both of the absorption and photoluminescence property of the complex **1** drastically changed in response to the formation of dimers (**1**)<sub>2</sub>. Homogeneous films were obtained by drop casting from the solution on solid surface, in which the interlocked dimers (**1**)<sub>2</sub> are densely accumulated. These unique self-assembly features of the trigonal complex **1** are distinct from the conventional  $\text{BF}_2\text{dk}$  complexes (**2–4**) that gave crystalline aggregates in  $\text{CHCl}_3$  and on the substrates. The present approach provides a new perspective in designing adaptive molecular coatings, which spread on surfaces without crystallization while maintaining high density of the functional groups. We presume that the present approach would be applicable to the design of functional interfaces such as light emitting layer for electroluminescence devices and sensory interfaces, where homogeneity and high density of functional groups are both required. Studies toward these applications are currently underway in these laboratories and will be reported in due course.

## Acknowledgements

This work was supported by a Grant-in-Aid for the Global COE Program, “Science for Future Molecular Systems” from the Ministry of Education, Culture, Sports, Science and Technology of Japan, a Grants-in-Aid for Scientific Research (S) (25220805) and by JST, CREST.

## Notes and references

- 1 a) T. F. A. De Greef, M. M. J. Smulders, M. Wolffs, A. P. H. J. Schenning, R. P. Sijbesma and E. W. Meijer. *Chem. Rev.*, 2009, **109**, 5687; b) Z. Chen, A. Lohr, C. R. Saha-Möllner and F. Würthner. *Chem. Soc. Rev.*, 2009, **38**, 564; c) C. Kulkarni, S. Balasubramanian and S. J. George. *ChemPhysChem*, 2013, **14**, 661; d) C. Rest, R. Kandanelli and G. Fernández. *Chem. Soc. Rev.*, 2015, **44**, 2543.
- 2 a) T. Kunitake. *Angew. Chem. Int. Ed.*, 1992, **31**, 709; b) T. Kawasaki, M. Tokuhiko, N. Kimizuka and T. Kunitake. *J. Am. Chem. Soc.*, 2001, **123**, 6792; c) Y. Tobe, N. Utsumi, K. Kawabata, A. Nagano, K. Adachi, S. Araki, M. Sonoda, K. Hirose and K. Naemura. *J. Am. Chem. Soc.*, 2002, **124**, 5350; d) T. Nakashima and N. Kimizuka. *Polym. J.*, 2012, **44**, 665.
- 3 a) A. R. A. Palmans, J. A. J. M. Vekemans, H. Fischer, R. A. Hikmet and E. W. Meijer. *Chem. Eur. J.*, 1997, **3**, 300; b) G.

- Hennrich, E. Cavero, J. Barberá, B. Gómez-Lor, R. E. Hanes, M. Talarico, A. Golemme and J. L. Serrano. *Chem. Mater.*, 2007, **19**, 6068; c) M. Lehmann and M. Jahr. *Chem. Mater.*, 2008, **20**, 5453; d) M. H. C. J. van Houtem, R. M-Rapún, J. A. J. M. Vekemans, E. W. Meijer. *Chem. Eur. J.*, 2010, **16**, 2258; e) A. Timme, R. Kress, R. Q. Albuquerque and H.-W. Schmidt. *Chem. Eur. J.*, 2012, **18**, 8329.
- 4 a) K. P. van den Hout, R. M-Rapún, J. A. J. M. Vekemans and E. W. Meijer. *Chem. Eur. J.*, 2007, **13**, 8111; b) M. M. J. Smulders, A. P. H. J. Schenning and E. W. Meijer. *J. Am. Chem. Soc.*, 2008, **130**, 606; c) F. García, J. Buendía and L. J. Sánchez. *Org. Chem.*, 2011, **76**, 6271; d) F. Aparicio, F. García and L. Sánchez. *Chem. Eur. J.*, 2013, **19**, 3239.
- 5 a) Y. Nishida, T. Tsurumi, K. Sasaki, K. Watanabe, H. Dohi and K. Kobayashi. *Org. Lett.*, 2003, **5**, 3775; b) M. K. Müller and L. Brunsveld. *Angew. Chem. Int. Ed.*, 2009, **48**, 2921; c) K. B. Joshi, K. V. Krishna and S. Verma. *J. Org. Chem.*, 2010, **75**, 4280; d) K. Matsuura, K. Watanabe, T. Matsuzaki, K. Sakurai and N. Kimizuka. *Angew. Chem. Int. Ed.*, 2010, **49**, 9662.
- 6 a) E. Congné-Laage, J.-F. Allemand, O. Ruel, J.-B. Baudin, V. Croquette, M. Blanchard-Desec and L. Jullien. *Chem. Eur. J.*, 2004, **10**, 1445; b) N. M. D. Brown and P. Blandon. *J. Chem. Soc. A*, 1969, 526; c) I. Sánchez, M. J. Mayoral, P. Ovejero, J. A. Campo, J. V. Heras, M. Cano and C. Lodeiro. *New J. Chem.*, 2010, **34**, 2937; d) M. J. Mayoral, P. Ovejero, M. Cano, and G. Orellana, *Dalton Trans.*, 2011, **40**, 377; e) B. Domercq, C. Grasso, J.-L. Maldonado, M. Halik, S. Barlow, S. R. Marder and B. Kippelen. *J. Phys. Chem. B.*, 2004, **108**, 8647; f) G. Zhang, J. Lu, M. Sabat and C.-L. Fraser. *J. Am. Chem. Soc.*, 2010, **132**, 2160.
- 7 a) X. Zhang, R. Lu, J. Jia, X. Liu, P. Xue, D. Xu and H. Zhou. *Chem. Comm.*, 2010, **46**, 8419; b) H. Maeda, Y. Haketa and T. Nakanishi. *J. Am. Chem. Soc.*, 2007, **129**, 13661; c) Y. Haketa, S. Sakamoto, K. Chigusa, T. Nakanishi and H. Maeda. *J. Org. Chem.*, 2011, **76**, 5177; d) C. Qian, M. Liu, G. Hong, P. Xue, P. Gong and R. Lu. *Org. Biomol. Chem.*, 2015, **13**, 2986.
- 8 a) I. Sánchez, J. A. Campo, J. V. Heras, M. Cano and E. Oliveira. *Inorg. Chim. Acta.*, 2012, **381**, 124; b) O. A. Turanova, A. N. Turanov, D. V. Lapaev, O. I. Gnezdilov, S. V. Lobkov and Yu. G. Galyametdinov. *Russ. J. Gen. Chem.*, 2006, **76**, 730.
- 9 G. Zhang, G. M. Palmer, M. W. Dewhirst and C.-L. Fraser. *Nat. Mater.*, 2009, **8**, 747.
- 10 a) D. Rohde, C.-J. Yan, H.-J. Yan and L.-J. Wan. *Angew. Chem. Int. Ed.*, 2006, **45**, 3996; b) D. Rohde, C.-J. Yan and L.-J. Wan. *Langmuir*, 2006, **22**, 4750.
- 11 L. Ronconi and P. J. Sadler. *Coord. Chem. Rev.*, 2008, **252**, 2239.
- 12 K. Ono, A. Nakashima, Y. Tsuji, T. Kinoshita, M. Tomura, J.-i. Nishida and Y. Yamashita. *Chem. Eur. J.*, 2010, **16**, 13539.
- 13 S. Madhu, M. R. Rao, M. S. Shaikh and M. Ravikanth. *Inorg. Chem.*, 2011, **50**, 4392.
- 14 R. B. Martin. *Chem. Rev.*, 1996, **96**, 3043.
- 15 M. Kasha, H. R. Rawls and M. A. El-Bayoumi. *Pure Appl. Chem.*, 1965, **11**, 371.
- 16 a) F. M. Winnik. *Chem. Rev.*, 1993, **93**, 587; (b) P. K. Lekha and E. Prasad. *Chem. Eur. J.*, 2011, **17**, 8609.
- 17 N. J. Turro. *Modern Molecular Photochemistry*, University Science Books, Sausalito, California, 1978.
- 18 W. West and S. Pearce. *J. Phys. Chem.*, 1965, **69**, 1894.
- 19 A. Foris. *Magn. Reson. Chem.*, 2004, **42**, 534.
- 20 J. Olmsted, III. *J. Phys. Chem.*, 1979, **83**, 2581.